12-1-2020

Evidence for Electron Energization Accompanying Spontaneous Formation of Ion Acceleration Regions in Expanding Plasmas

Evan M. Aguirre
West Virginia University

Rikard Bodin
Gettysburg College

Neng Yin
Gettysburg College

Timothy N. Good
Gettysburg College

Earl E. Scime
West Virginia University

Follow this and additional works at: https://cupola.gettysburg.edu/physfac

Part of the Physical Processes Commons, and the Plasma and Beam Physics Commons

Share feedback about the accessibility of this item.

Evidence for Electron Energization Accompanying Spontaneous Formation of Ion Acceleration Regions in Expanding Plasmas

Abstract

We report experiments conducted in an expanding argon plasma generated in the inductive mode of a helicon source in the Hot hELIcon eXperiment−Large Experiment on Instabilities and Anisotropies facility. As the neutral gas pressure increases, the supersonic ion acceleration weakens. Increasing neutral pressure also alters the radial profile of electron temperature, density, and plasma potential upstream of the plasma expansion region. Langmuir probe measurements of the electron energy probability function (EEPF) show that heating of electrons at the plasma edge by RF fields diminishes with increasing gas pressure, yielding a plasma with a centrally peaked electron temperature, and flat potential profiles at higher neutral pressures. For neutral pressures at which ion acceleration regions develop in the expanding plasma plume, EEPFs reveal electrons with two temperature components.

Keywords

Plasma thruster, ion acceleration in a diverging magnetic field

Disciplines

Physical Processes | Physics | Plasma and Beam Physics

Evidence for electron energization accompanying spontaneous formation of ion acceleration regions in expanding plasmas

E. M. Aguirre, R. Bodin, N. Yin, T. N. Good, and E. E. Scime

COLLECTIONS

View Online   Export Citation   CrossMark

ARTICLES YOU MAY BE INTERESTED IN

Evidence for electron energization accompanying spontaneous formation of ion acceleration regions in expanding plasmas ⓔⓟ

View Online   Export Citation   CrossMark

E. M. Aguirre,[1,a)] ⓘⒹ R. Bodin,[2] ⓘⒹ N. Yin,[2] T. N. Good,[2] and E. E. Scime[1] ⓘⒹ

AFFILIATIONS

[1]Department of Physics, West Virginia University, Morgantown, West Virginia 26505, USA
[2]Department of Physics, Gettysburg College, Gettysburg, Pennsylvania 17325, USA

[a)]Author to whom correspondence should be addressed: emaguirre@mix.wvu.edu

ABSTRACT

We report experiments conducted in an expanding argon plasma generated in the inductive mode of a helicon source in the Hot hELIcon eXperiment–Large Experiment on Instabilities and Anisotropies facility. As the neutral gas pressure increases, the supersonic ion acceleration weakens. Increasing neutral pressure also alters the radial profile of electron temperature, density, and plasma potential upstream of the plasma expansion region. Langmuir probe measurements of the electron energy probability function (EEPF) show that heating of electrons at the plasma edge by RF fields diminishes with increasing gas pressure, yielding a plasma with a centrally peaked electron temperature, and flat potential profiles at higher neutral pressures. For neutral pressures at which ion acceleration regions develop in the expanding plasma plume, EEPFs reveal electrons with two temperature components.

Published under license by AIP Publishing. https://doi.org/10.1063/5.0025523

I. INTRODUCTION

During the past 15 years, much effort has been focused on understanding why expanding helicon sources spontaneously produces a supersonic ion beam population at low pressure. This discovery has impacted plasma thrusters,[1,2] space plasmas,[3] and magnetic reconnection[4] research. These ion beams have been produced in various gases[5,6] and for a wide range of plasma source parameters.[7]

Initial studies suggested that the ion beams were created by spontaneous formation of a double layer (DL).[8,9] A classic DL is a structure composed of two oppositely charged layers that support highly localized electric fields. A DL is a freestanding structure that can appear anywhere in a plasma. In expanding helicon plasmas, the ion acceleration occurs in the transition region from the plasma source to the expansion chamber.[10] This region also coincides with a steep drop in the magnetic field and in the plasma density. Many studies focused solely on the plasma upstream or downstream of the acceleration region.[11] However, experiments that managed to study the length of the accelerating region found that it was not a few Debye lengths long, as would be expected for a DL, but many hundred Debye lengths long.[12] Recent experiments in our experimental facility found evidence that the accelerating structure is not a true DL.[13] Other groups that have succeeded in performing measurements throughout the

acceleration region also report structures on the order of 1000 Debye lengths long and have arrived at this similar conclusion regarding the ion beam formation process.[14]

The critical role of neutral pressure in spontaneous ion beam formation has been known since the initial discovery.[8] Formation of ion beams in expanding plasmas typically requires a neutral pressure no greater than 2–3 mTorr.[13] A decrease in the downstream neutral pressure results in an increase in the ion beam velocity when all other parameters are held fixed.[9,15] The work by Zhang *et al.*[15] clearly established that the accelerating structure, specifically the location of an ion hole (a region of localized negative potential in which a population of ions is trapped and there is a plasma density decrease) is constrained to the diverging magnetic field and shifts radially inward with increasing downstream neutral pressure. Other work in our facility that focused on multi-gas plasmas yielded insights into the role of partial pressure of different gases and collisionality of the plasma.[6]

As studies of spontaneous ion beam formation have matured, many groups have reported observations of hot, high energy electrons streaming from the plasma source into the expansion region at the same time the ion beams appear. Work on the MadHex facility identified two electron temperature populations within the plasma.[16,17] The hot population was downstream of the accelerating structure, while

the cooler population was trapped upstream. Takahashi *et al.* observed hot electrons traveling along magnetic field lines into a magnetic nozzle.[18] Takahashi *et al.* proposed two possible explanations for the energetic electrons: RF skin heating effects in the source and energization by plasma instabilities. Takahashi *et al.* ruled out instabilities, consistent with our studies which also suggested RF skin effects were heating the electrons in the plasma edge. The skin effect hypothesis suggests a new paradigm for ion beam formation in expanding plasmas.[13] The ions are accelerated because energetic electrons created at the edge of the plasma (a few skin depths into the plasma) stream downstream and through the expansion regions with few collisions. To enforce quasineutrality, a spatially distinct region of ion acceleration (inside of the annulus of energetic electrons) must arise through ambipolar fields. The result is a long (hundreds of Debye lengths long), cylindrical, well-confined, ion acceleration region that is surrounded by a ring of energetic electrons.

The existence of hot, high energy electrons in expanding helicon plasmas is now reasonably well established.[19] However, great care must be undertaken in the analysis of electron energy probability function (EEPF) or electron energy distribution function (EEDF) measurements in the noisy RF environment of a helicon source; whether the measurements are obtained from a Langmuir probe or a retarding field energy analyzer (RFEA). The distributions are non-Maxwellian and claims of two electron temperature populations depend strongly on the analysis method. The very phrase "two electron temperature population" is problematic because it has two different meanings. The first is that there are two electron populations in different spatial regions each with a distinct temperature, as in the case of MadHex. The second is that a distribution has two populations (i.e., a cool and hot component).

Because some DL formation models are also based on the existence of two-component electron populations, there remains some debate about the ion acceleration process. Is it just an ambipolar field created by energetic electrons, or is it a DL created by the energetic electrons? Singh's review provides an excellent summary of the variety of mechanisms that result in a DL.[20] The two-electron temperature-current free double layer (TET-CFDL), is a phenomenon primarily seen in space plasmas. This mechanism requires $T_h > 10 T_c$ and results in parallel charge separation that drives ion acceleration (not the perpendicular charge separation now reported in laboratory helicon plasmas). The break energy[21] or the existence of electrons with two temperature components shows where particles are trapped in the plasma. A lower T_e at higher energy signals particle depletion and is a proxy for separation of electrons into trapped and passing populations in the presence of the accelerating structure.[22,23] A radial transport barrier develops which is correlated with the acceleration of ions downstream.[24]

Based on the current research described above, there is a gap in understanding exactly how the energetic electrons are produced and how they influence/create the ion beam. Together with our previous work, these observations motivated further study into the role of neutral pressure and energetic electrons on ion beam formation. To explore the relationship of the details of the EEPF and ion acceleration in expanding plasmas, we present radial profiles of the EEPF and effective electron temperature at various neutral pressures for which significant ion acceleration is also observed. We also investigate the effects of electrons in specific energy ranges (in bins of 10 eV) by presenting radial profiles of the electron density of each energy range normalized to the total electron density.

II. EXPERIMENTAL APPARATUS AND METHODS

These experiments were performed in (see Fig. 1) the Hot hELIcon eXperiment (HELIX) and the Large Experiment on Instabilities and Anisotropies (LEIA). HELIX is a 1.5 m long hybrid stainless steel-Pyrex vacuum chamber. The diameter of the Pyrex chamber is 10 cm, while the stainless-steel chamber diameter is 15 cm. The stainless-steel chamber opens up into the 1.8 m inner diameter, 4.5 m long (LEIA) expansion chamber. RF power is coupled through a 19 cm $m = +1$ helical antenna over a frequency range of 8–18 MHz. A uniform, axial magnetic field of 0–1200 G in the plasma source is produced by ten water cooled electromagnets. In the expansion region, seven water cooled electromagnets produce a steady-state, uniform axial magnetic field of 0–150 G. Three turbomolecular drag pumps provide a base pressure of approximately 10^{-8} Torr. The large pumping rate at the end of the expansion chamber yields a downstream pressure much smaller than the neutral pressure in the source. A more detailed description of the HELIX–LEIA facility is available elsewhere.[25]

For these experiments, the neutral fill pressure of argon was varied between 0.11 mTorr and 1 mTorr. At those neutral pressures, the mean free path for ion-neutral charge exchange collisions is a few cm. The antenna frequency was 12.5 MHz and 725 W of total RF power, with less than 20 W reflected. The magnetic field in the source was 860 G and the downstream LEIA magnetic field was 108 G.

Only a brief overview of LIF is given here as LIF provides the ion beam velocity measurements in the downstream plasma. LIF is a non-perturbative diagnostic that uses the Doppler effect to directly measure the thermally broadened ion velocity distribution function (IVDF). For Ar II LIF, a Matisse-DR (Dye Ring) tunable ring dye laser is tuned to 611.6616 nm (vacuum wavelength) to pump the Ar II $3d^2 G_{7/2}$ metastable state to the $4p^2 F_{7/2}$ state, which then decays to the $4s^2 D_{5/2}$ state by emitting 461.086 nm photons. Approximately 10% of the laser light is diverted to a wavemeter (Bristol 621) and an iodine cell for absolute wavelength measurements. The remaining laser light passes through an optical diode to prevent reflections and then a mechanical
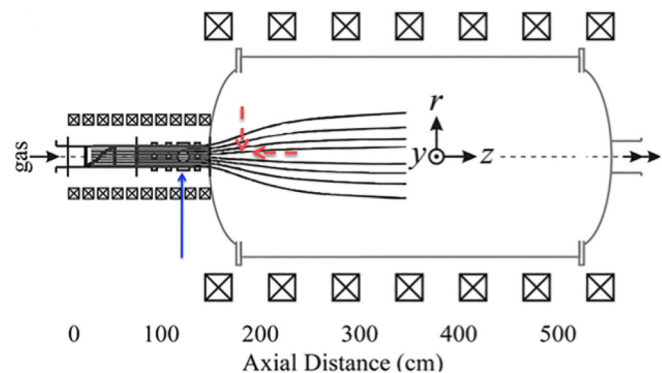

FIG. 1. The magnetic field geometry as the plasma expands from the helicon source into the LEIA chamber. The LIF measurements occur at the intersection of the two dashed red arrows. The solid blue arrow represents the location of Langmuir measurements. Adapted with permission from Aguirre *et al.*, Phys. Plasmas **24**, 123510 (2017). Copyright 2017 American Institute of Physics.

chopper operating at 5 kHz. The light is coupled into an optical fiber for injection into the plasma. Fluorescent emission is also collected by the optical fiber and the collected light passes through a narrowband filter (1 nm) before being measured with a photo-multiplier tube. As the laser's wavelength is scanned, the intensity of the fluorescence is measured with a lock-in amplifier to isolate the modulated (5 kHz) fluorescence. Detailed descriptions of the full LIF system are available elsewhere.[19] The laser injection and the fluorescent emission collection are accomplished with an *in situ*, scanning, mechanical probe.

The Langmuir probe used in this study consists of a 500 μm graphite tip, sheathed with an alumina tube, with an exposed length of $\sim$2 mm. The probe easily withstands months of exposure to the steady-state plasma. The probe is RF compensated via a series of RF "chokes," which are self-resonant inductors, and a 10 nF tantalum capacitor. One side of the capacitor is attached to the probe tip and the other end is floating but entirely encased in the insulating probe housing. This arrangement effectively short-circuits the high frequency fluctuations of the probe tip. The inductors have a large impedance for a wide range of antenna frequencies (HELIX is a variable frequency helicon source) to provide additional attenuation of the RF fluctuations. A frequency response test was conducted on the Langmuir probe which showed excellent attenuation across the antenna frequencies typically used in the source. Additional details on the frequency response test, along with construction of the Langmuir probe, are described elsewhere.[26]

Simple Langmuir probe analysis is rarely sufficient in RF plasmas, especially for non-Maxwellian distribution functions. Using a more detailed analysis method, it is possible to construct the EEDF, f_e, or the EEPF, f_p. The plasmas described here are not completely in thermodynamic equilibrium, therefore they are inherently non-Maxwellian. The low energy portion of the electron distribution is consistent with inelastic collisions with neutrals not playing a significant role in determining the details of the electron distribution function. Unusual for a helicon source, the ionization fraction is low because we are not in a high field, high RF power regime. The ionization fraction falls from the center of the plasma to only 0.001–0.01 at the plasma edge.[27] Therefore, the EEPF is obtained from a Druyvesteyn analysis. The generalized electron current from the Langmuir probe is given by[28]

$$I_e = \frac{eA_p}{\sqrt{8m_e}} \int_{eU}^{\infty} \frac{(E - eU)f_p(E)}{1 + [(E - eU)/E]\Psi(E)} \, dE, \quad (1)$$

where A_p is the probe area, $f_p(E)$ is the EEPF, and $U = |V - V_p|$ such that $E = eU$. $\Psi(E)$ is the diffusion parameter defined as[29,30]

$$\Psi(E) = \frac{r_p}{\gamma \rho_e(E)} \ln\left(\frac{\pi l_p}{4 r_p}\right). \quad (2)$$

Equation (2) depends on the length of the probe tip l_p and a unitless geometric factor, $\gamma = 4/3 - 0.62 \exp(-\lambda_e/2r_p)$, based on the energy dependent electron gyroradius, ρ_e, the electron momentum loss scale length, λ_e, and the probe radius r_p.

There are three analysis regimes depending on the value of Ψ. For the experiments in this work, $\Psi \sim 7$ and $f_p \propto dI_e/dU$. In this regime, the probe collects electrons tied to the field lines that intersect the probe surface. The EEPF is found from the first derivative of the probe current

$$\frac{dI_e}{dU} = \frac{eA_p}{\sqrt{8m_e}}\left[\frac{eU}{\Psi}f_p(E) + \int_{eU}^{\infty} \frac{Ef_p(E)}{(1+\Psi)[(1+\Psi)E - \Psi eU]} \, dE\right]. \quad (3)$$

The EEPF is then[28,29]

$$f_p(E) = \frac{3\gamma\sqrt{2m_e}}{2e^3 A_p} \frac{\Psi}{U} \frac{dI_e}{dU}. \quad (4)$$

The electron temperature and density are then calculated by taking moments of the distribution function. The electron density is

$$n_e = \int_{E_1}^{E_2} E^{1/2} f_p(E) dE, \quad (5)$$

where E_1 and E_2 are the lower and upper energy values of interest, respectively, and f_p has units of eV$^{-3/2}$ m^{-3}. The effective electron temperature is

$$T_e = \frac{2}{3}\langle E \rangle = \frac{2}{3}\left[\frac{1}{n_e}\int_{E_1}^{E_2} E^{3/2} f_p(E) dE\right]. \quad (6)$$

When $E_1 = 0$ and $E_2 = \infty$, Eqs. (2) and (3) give the total electron density and corresponding temperature. The temperature (in eV) is defined in terms of the mean energy of the distribution as opposed to the distribution width. The temperature defined here is a temperature based on the energy range of interest. An example EEPF showing two temperature components is shown later to illustrate this analysis. Similar results are obtained from linear fits to semilog plots of the EEPF over the energy range of interest. The plasma potential V_p is the voltage of maximum $\frac{dI_e}{dV}$ or the zero crossing of $\frac{dI_e^2}{dV^2}$. In an EEPF, a Maxwellian distribution appears as a linear function, while a non-Maxwellian distribution has a variety of features.

At low pressure, the Langmuir data are quite noisy. Therefore, we have smoothed the data at each step of the analysis (i.e., smoothing I_e, $\frac{dI_e}{dU}$, and finally $f_p(E)$) while minimizing induced errors. For the data presented here, a Blackman filter was used because of its advantages for noisier data.[31] Additional information on the smoothing methods used is given in the literature.[26]

III. MEASUREMENTS AND DISCUSSION

Radial profiles of the plasma potential, energy-dependent electron temperature, and EEPF were measured at $(r, z) = (r, 112)$ cm. This location, shown in Fig. 1 at the blue arrow, is approximately 50 cm downstream from the antenna and 47 cm upstream from the plasma source/expansion chamber junction. The parallel IVDFs as a function of pressure were measured at $(r, z) = (0, 170)$, 11 cm downstream of the plasma source/expansion chamber junction (shown in Fig. 1 at the intersection of the two dashed red arrows). All measurements at a neutral pressure of $p = 0.11$ mTorr were reported previously.[13] Five Langmuir probe traces were averaged for the $p = 0.11$ mTorr measurements, while twenty-five were averaged for all other neutral pressures.

The ion beam velocity, measured with LIF, is shown in Fig. 2 and Table I as a function of neutral pressure. Figure 2 is adapted from our previous work[6] where each IVDF is normalized to its maximum amplitude for clarity and plotted as a contour. We have overlapped our most recent LIF measurements as black squares to show
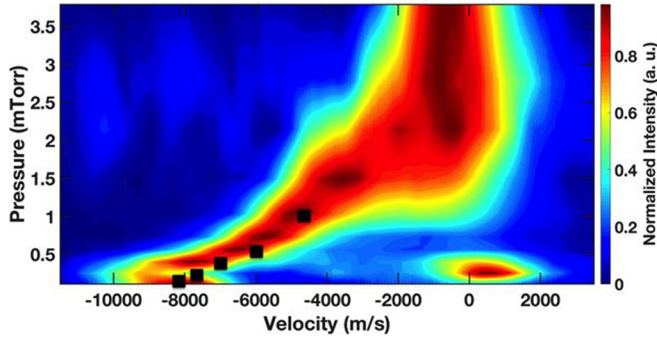
FIG. 2. The parallel IVDFs measured with LIF with the ion beam velocity measured in this work marked as a black square. Each IVDF is normalized to its maximum amplitude and plotted as a contour. Adapted with permission from Aguirre *et al.* Phys. Plasma **25**, 043507 (2018). Copyright 2018 American Institute of Physics.

reproducibility. There is a slight difference in ion beam velocity between the two datasets which is due to the different measurement locations ($(r, z) = (0, 164)$ cm for our previous work and $(r, z) = (0, 170)$ cm here). For a pressure of $p = 0.11$ mTorr, the ion beam velocity is 8.3 km/s but slows to 4.5 km/s as neutral pressure increases to $p = 0.90$ mTorr. The values reported here follow the same trend as reported previously.[6] The ion beam at $p = 0.11$ mTorr is quite distinct in the IVDF measurements because it is fast, large amplitude, and its radial diameter in the downstream plasma is 10 cm. As the pressure increases, the beam amplitude and bulk velocity decrease even though the ion beam remains supersonic for all neutral pressures.

To determine the electron temperature from the EEPF, a linear fit was used for the low energy (15–35 eV) and high energy ($>$35 eV) electrons of the EEPF. For large radial positions, the EEPFs consist of two electron populations [see Fig. 3(a)]. Higher temperatures are obtained from analysis of the low energy electron population (shown in red) and lower temperatures are obtained from analysis of the high energy electrons (shown in blue). A perfectly Maxwellian distribution has only one, well-defined temperature as shown in Fig. 3(b). The electron temperature across the plasma radius as a function of pressure is shown in Fig. 4(a). At the lowest pressure, both populations exhibit a peak in temperature from 3 cm $< r <$ 4 cm. For low pressures and in the center of the plasma, the EEPFs are mostly Maxwellian [see Fig. 3(b)] and therefore, the temperatures determined from the two populations are nearly equal. As the pressure increases, the radial profile of the temperature of the high energy electrons flattens. The maximum

TABLE I. Summary of the variation of ion beam velocity, electron skin depth ($\delta = c/\omega_{pe}$), effective electron skin depth ($\delta_{eff} = \left(\frac{v_{th,e}c^2}{\omega_{RF}\omega_{pe}^2}\right)^{1/3}$), and electron quiver distance during an RF period normalized to the collisionless skin depth ($v_{th,e}/\delta\omega_{RF}$).

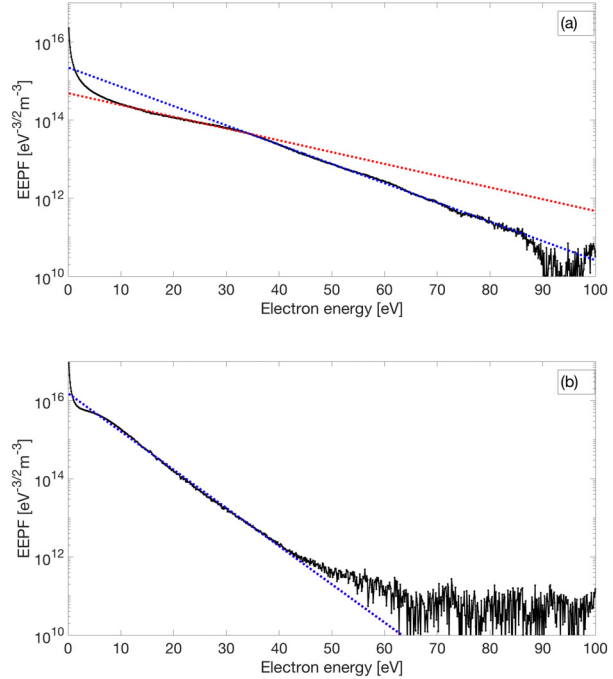| Pressure (mTorr)	v_{beam} (km/s)	δ_{eff} (cm)	δ (cm)	$v_{th,e}/\delta\omega_{RF}$
0.11	8.3 ± 0.15	1.89	1.87	1.02
0.25	7.8 ± 0.15	1.28	1.11	1.54
0.40	6.8 ± 0.15	1.04	0.83	1.94
0.56	6.0 ± 0.15	0.95	0.82	1.51
0.90	4.5 ± 0.15	0.79	0.65	1.74

FIG. 3. (a) EEPF at $r = 4.5$ cm and $p = 0.11$ mTorr showing two temperature components. The break energy is defined as the energy at which these two components intersect. Note that the lower energy electron population exhibits a larger temperature than the high energy population. (b) EEPF at $r = 0$ cm and $p = 0.11$ mTorr showing a mostly Maxwellian plasma.

electron temperature, derived from the lower energy electrons decreases with increasing pressure until the profile changes completely. At the highest neutral pressure, the lower energy electron temperature is peaked in the center and decreases outside the central, core region of the plasma. Collisional transport of particles and energy in a cylindrical system naturally leads to a peaked density and temperature profile if plasma is created throughout the plasma column and the axial transport is comparable to radial transport.

The plasma potential was determined from the inflection point of the Langmuir probe I–V curve and is shown as a function of r in Fig. 5(a). For a pressure of 0.11 mTorr, resulting in a strong ion beam, the radial plasma potential profile shows an electron-rich/ion deficient region (ion hole) located at $r = 3$ cm. The ion hole persists for pressures up to $p = 0.40$ mTorr but the plasma potential in the region 3 cm $< r <$ 4 cm does not change significantly. At the highest pressures, the radial plasma potential profile flattens and an ion beam is still observed downstream. Therefore, downstream ion beam formation is contingent on more than just an upstream hollow feature in the plasma potential or overall plasma density.

As shown in Fig. 6, the EEPFs, obtained using the Druyvesteyn method, provide detailed information regarding the density of electrons in particular energy ranges across the plasma column. The density of electrons in each energy range is normalized to the total electron density at each radial location. The lowest energy electrons ($<$20 eV) are omitted from the analysis to focus attention on the higher energy electrons. As the neutral pressure increases, the total
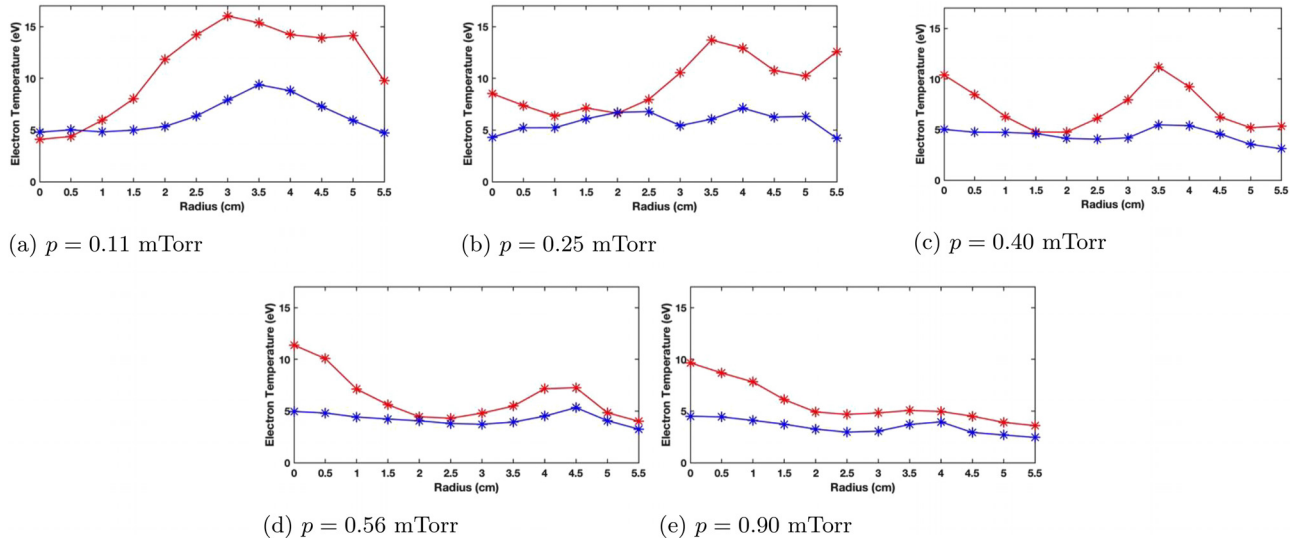
FIG. 4. Radial profiles of the electron temperature for the high energy electrons (blue) and low energy electrons (red) for (a) $p = 0.11$ mTorr, (b) $p = 0.25$ mTorr, (c) $p = 0.40$ mTorr, (d) $p = 0.56$ mTorr, and (e) $p = 0.90$ mTorr.

electron density and fraction of the electron distribution with energies (>20 eV) on axis increase, i.e., the normalized densities of each energy band increase. For example, the normalized density of the 50–60 eV band increases from less than 0.0001 at $p = 0.11$ mTorr to nearly 0.01 at $p = 0.56$ mTorr at $r = 0$ cm. The radial profiles of the two highest energy bands (40–50 eV and 50–60 eV) exhibit the clearest evidence of RF heating in the edge that decreases with increased pressure. At the lowest pressure, $p = 0.11$ mTorr, both profiles have a broad peak centered on $r = 3.5$ cm and a clear peak in normalized density. As the neutral pressure increases, the relative fraction of the electron population at the plasma edge in those energy bands decreases by nearly an

order of magnitude from $p = 0.11$ mTorr to $p = 0.90$ mTorr. The width of the region of enhanced densities in those energy bands also decreases with increasing pressure. Therefore, as the neutral pressure increases and the downstream ion beam weakens and slows down, the fraction of electrons in the most energetic electron population at the plasma edge also decreases.

However, the enhancement in the EEPF at higher energies does not completely go away at the highest pressures. Shown in Fig. 7 are the EEPFs for $p = 0.90$ mTorr. While the EEPF is well described by a two Maxwellian population at $r = 0$ cm, at larger radial positions, a distinct peak in the EEPF around 20 eV is clearly evident. At lower
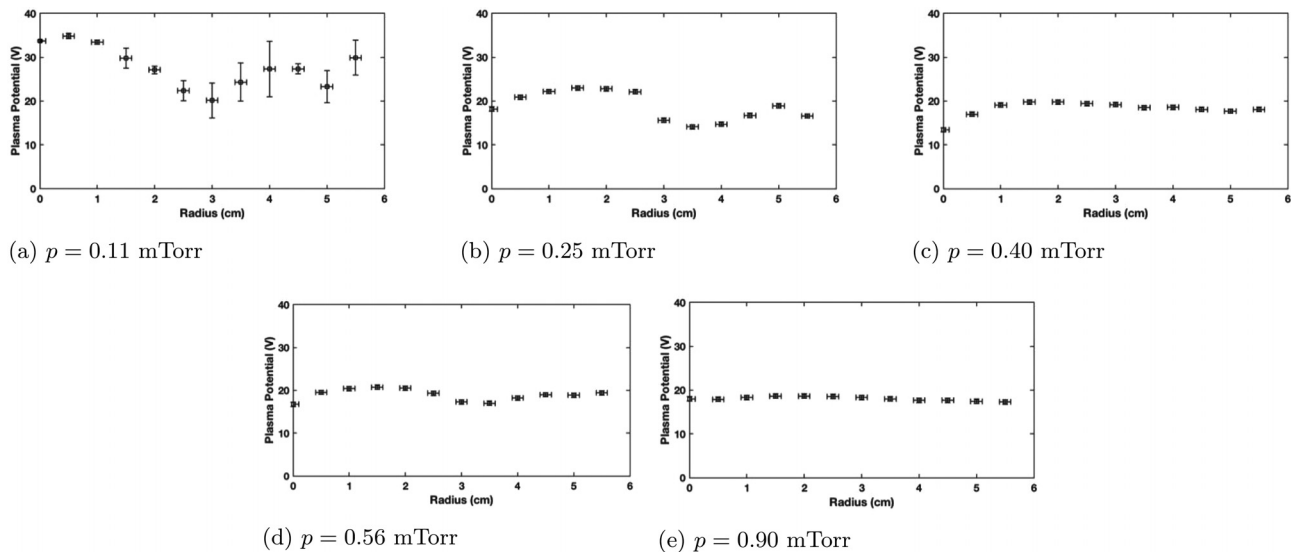

FIG. 5. The plasma potential across the plasma column for (a) $p = 0.11$ mTorr, (b) $p = 0.25$ mTorr, (c) $p = 0.40$ mTorr, (d) $p = 0.56$ mTorr, and (e) $p = 0.90$ mTorr.
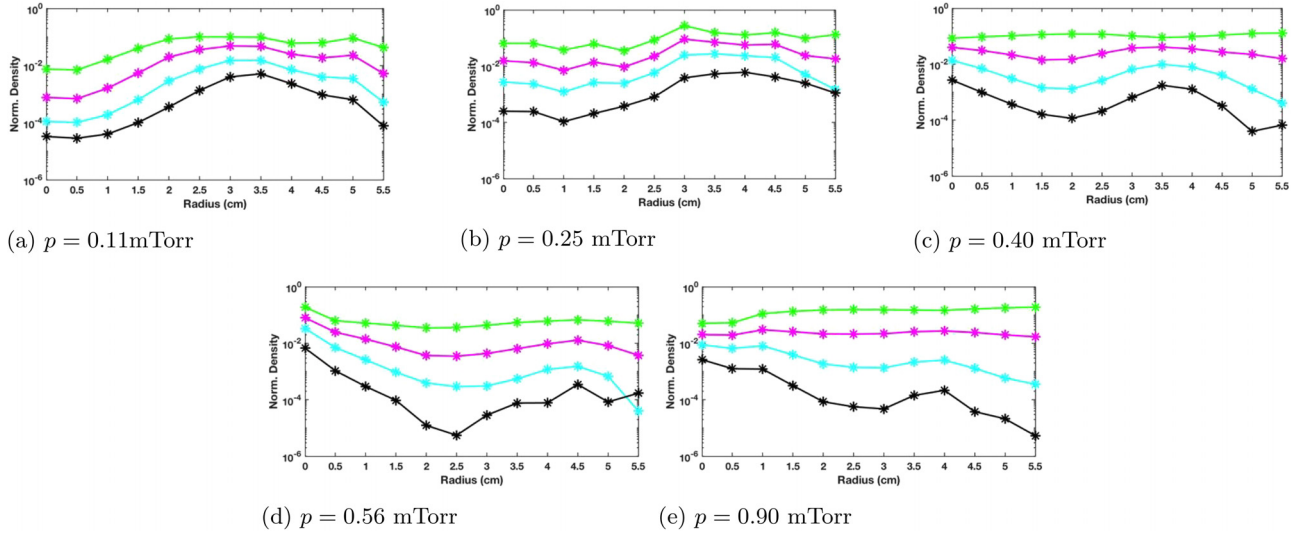
FIG. 6. The density of 20–30 eV (green), 30–40 eV (magenta), 40–50 eV (cyan), and 50–60 eV (black) electrons normalized to the total electron density across the plasma column for (a) $p = 0.11$ mTorr, (b) $p = 0.25$ mTorr, (c) $p = 0.40$ mTorr, (d) $p = 0.56$ mTorr, and (e) $p = 0.90$ mTorr.

pressures, the "beam" in the EEPFs is much more pronounced for radial positions further from the axis, i.e., the broad enhancement in Fig. 6(a) for all energy ranges. There is still broad energization at a pressure of $p = 0.40$ mTorr as evidenced by the EEPFs in Fig. 8. The electron energization begins to shift at this pressure from a broad enhancement to primarily high energy enhancement. We should also note that the electron beam energy does not change with pressure (see Figs. 7 and 8), so it is not an indicator of the strength of the ion accelerating structure. The beam energy does not correlate with the break energy when there are trapped and streaming electron populations either.

Our previous studies,[13] along with those of other groups,[18] implicated the RF skin effect as a possible mechanism for generating energetic electrons at the edge of these plasmas. Relatively low frequency ($f_{RF} \sim 10$ MHz) electromagnetic waves such as the helicon wave cannot propagate across the plasma column since $\omega_{RF} < \omega_{pe}$ ($7.85 \times 10^7 < (1-5) \times 10^{10}$) rad/s. However, at the edge where the plasma density drops (within a skin depth), the RF wave

from the helicon antenna may directly interact with electrons. There are two standard methods of calculating the RF skin depth.[32] The first is to calculate the simple, unmagnetized, collisionless skin depth given by

$$\delta = c/\omega_{pe}, \qquad (7)$$

which is valid for $\omega < \omega_{pe}$ (or $\nu_{en} \ll \omega$), where $c = 3 \times 10^8$ m/s is the speed of light, $\omega_{pe} = (1.6 - 4.6) \times 10^{10}$ rad/s is the electron plasma frequency, and $\nu_{en} = (8.2 - 25.0) \times 10^5$ s^{-1} is the electron–neutral collision frequency. For the plasmas in this experiment, the dominant collisions are electron–neutral and ion–neutral collisions. The collisionless skin depth at each pressure is given in Table I. As the neutral pressure increases, the plasma density and the skin depth decrease from nearly 2 cm to roughly 0.5 cm. These scales are roughly consistent with the widths of the energetic electron density enhancements seen in Fig. 6.

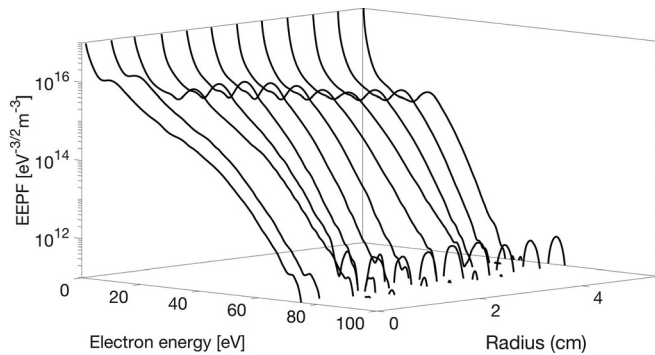The second method is to calculate the anomalous skin depth as defined by

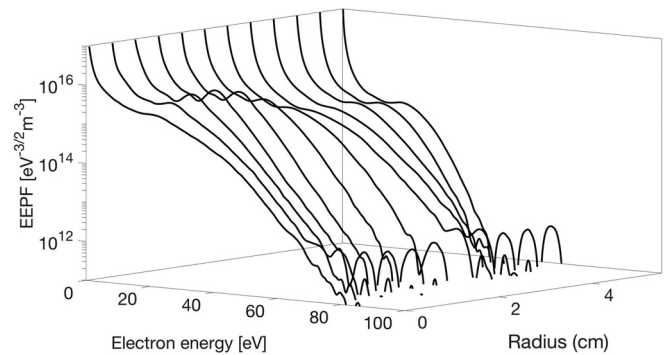**FIG. 7.** The EEPFs across the radius of the plasma for $p = 0.90$ mTorr.

FIG. 8. The EEPFs across the radius of the plasma for $p = 0.40$ mTorr.

$$\delta_{eff} = \left(\frac{v_{th}c^2}{\omega_{RF}\omega_{pe}^2} \right)^{1/3}, \tag{8}$$

where c is the speed of light and v_{th} is the electron thermal speed. The anomalous skin depth is valid for plasma for which Ohmic heating does not dominate.[32] For these plasmas, the anomalous skin depth is a more correct calculation since an electron moves through the RF layer within a time shorter than the RF period, as evidenced by the values of the ratio $v_{th,e}/\delta\omega_{RF}$ given in Table I.[32] When $v_{th,e} > \omega\delta$, as in this study, non-local electrodynamics become important.[33] As shown in Table I, the anomalous skin depth calculation results in only modest corrections to the classic skin depth values. Based on the radial extent of the electron heating shown in Fig. 4(a) and energetic electrons shown in Fig. 6, either skin depth calculation is adequate. However, assuming that the collisionless skin depth is adequate ignores these important effects.

It is clear that at all pressures investigated, some electrons are energized at the edge of the plasma. At low pressure, electrons of all energies are heated at the plasma edge, but as the pressure increases, only the highest energy electrons exhibit some edge heating. As the pressure increases, the source plasma also begins to transition from an inductive mode to a classic "blue" core helicon mode. The radial profile of the electron temperature profile shows this transition the most clearly. Below $p = 0.40$ mTorr, the plasma exhibits a two temperature population with a peak in heating toward the plasma edge. Above $p = 0.40$ mTorr, the plasma transitions to a more conventional helicon mode plasma with centrally peaked electron temperature and plasma density profiles. Given that the slow wave, Trivelpiece-Gould (TG) mode, is strongly damped at the plasma edge for all plasma densities[34] and neutral pressures and the fast wave (helicon mode) is able to propagate to the core once the plasma density reaches a value capable of supporting helicon waves, it seems plausible that the bulk heating of electrons in the plasma core at higher pressures by the helicon wave is responsible for the core electron heating observed here. Niemi and Krämer[35] also identified heating of bulk electrons by the fast wave in the core—at pressures comparable to the higher pressures used in this work. Thus, a plasma core with hot bulk electrons and cool tail electrons might be an indicator of fast wave heating.[36] More recent work by Piotrowicz et al.[37] measured the edge-to-core power coupling transition, although in a light–ion helicon source. The edge-to-core electron heating and density production is also dependent on the unmagnetized ions via a short circuit effect.[38,39] A number of researchers have searched for, and some have reported measurements of, a specific population of electrons in resonance with the helicon wave in helicon source plasmas.[33,40] The pronounced "bump" in the EEPFs shown in Figs. 7 and 8 is certainly suggestive of such a collisionless wave-particle resonance process and the energy of the feature is consistent with those earlier reports. As the pressure increases and the plasma transitions modes, this feature encompasses most of the plasma column (see Fig. 7) Why the feature shifts in energy with increasing radial position is not understood.

Because the high energy electron population at the plasma edge, and the downstream ion beam, persist for all neutral pressures investigated here, the hypothesis that edge electron heating creates an energetic electron population that travels downstream along the expanding magnetic field and sets up an ambipolar potential that then accelerates the ions out of the plasma core is entirely consistent with these observations. Because $T_h > 10T_c$ is never satisfied, even the TET-CFDL formation mechanism described by Singh would never arise.

It is worth noting that as the pressure increases, and the ion beam slows, the ion hole decreases in magnitude until it disappears. Even though the ion hole disappears at high pressure at the measurement location, an ion beam and ion hole are still detected downstream with concurrent observations of electron energization at the plasma edge upstream.[13] Since our Langmuir measurement location is between the antenna and the LIF measurement location, this suggests that the ion accelerating structure shifts downstream consistent with previous experiments and modeling results.[41,42]

IV. CONCLUSION

Our results are entirely consistent with RF skin effects creating local electron heating and energy deposition. Even at higher neutral pressures, when the density profile becomes centrally peaked, electrons continue to be heated within a few skin depths of the plasma edge, while the core electron temperature also increases significantly. Most importantly, our results link the changing coupling of the helicon source—i.e., the electron energization, to the strength of the ion acceleration measured in expanding plasmas.

The observations presented here point to a new understanding of the mechanism behind ion acceleration in expanding helicon plasmas. Pressure is the barrier to energetic electrons penetrating into the plasma core because of wave damping and collisions in the plasma edge. Energetic electrons appearing in the plasma core may provide evidence for fast wave propagation across the plasma column and subsequent coupling to the electrons.[43,44] The energy of the downstream ion beam created by quasineutrality requirements depends on the density (and energy) of the energetic electrons created in the plasma edge and collisional slowing of the ions. As the pressure increases, the ion acceleration region shifts downstream and might therefore result in less time for ions to accelerate before they are measured downstream. The radial structure in the energetic electron population is consistent with the anomalous skin depth of the RF wave. Future work on helicon sources could provide unequivocal evidence of the edge-to-core mechanism and its impact on the spontaneous ion acceleration. These scattering measurements[45] could observe the slow wave fluctuations while simultaneously monitoring the effects described here.

DATA AVAILABILITY

The data that support the findings of this study are available from the corresponding author upon reasonable request.

REFERENCES

[1]T. Lafleur, Phys. Plasmas **21**, 043507 (2014).
[2]J. L. Ferreira, F. N. de Oliveira, E. G. Costa, H. de Oliveira, Jr., and A. C. Branco, J. Phys. **641**, 012024 (2015).
[3]R. E. Ergun, L. Andersson, J. Tao, V. Angelopoulos, J. Bonnell, J. P. McFadden, D. E. Larson, S. Eriksson, T. Johansson, C. M. Cully, D. N. Newman, M. V.

Goldman, A. Roux, O. LeContel, K.-H. Glassmeier, and W. Baumjohann, Phys. Rev. Lett. **102**, 155002 (2009).

[4] J. Egedal, W. Daughton, A. Le, and A. L. Borg, Phys. Plasmas **22**, 101208 (2015).

[5] C. Charles, Appl. Phys. Lett. **84**, 332–334 (2004).

[6] E. M. Aguirre, E. E. Scime, and T. N. Good, Phys. Plasmas **25**, 043507 (2018).

[7] C. Charles, Plasma Sources Sci. Technol. **16**, R1–R25 (2007).

[8] C. Charles and R. Boswell, Appl. Phys. Lett. **82**, 1356–1358 (2003).

[9] X. Sun, C. Biloiu, R. Hardin, and E. E. Scime, Plasma Sources Sci. Technol. **13**, 359–370 (2004).

[10] F. Chen, Phys. Plasmas **13**, 034502 (2006).

[11] S. C. Thakur, Z. Harvey, I. A. Biloiu, A. Hansen, R. A. Hardin, W. S. Przybysz, and E. E. Scime, Phys. Rev. Lett. **102**, 035004 (2009).

[12] X. Sun, A. Keesee, C. Biloiu, E. Scime, A. Meige, C. Charles, and R. W. Boswell, Phys. Rev. Lett. **95**, 025004 (2005).

[13] E. M. Aguirre, D. S. Thompson, E. E. Scime, and T. N. Good, Phys. Plasmas **24**, 123510 (2017).

[14] A. Bennet, C. Charles, and R. Boswell, Phys. Plasmas **25**, 023516 (2018).

[15] X. Zhang, E. M. Aguirre, D. S. Thompson, J. McKee, M. Henriquez, and E. E. Scime, Phys. Plasmas **25**, 023503 (2018).

[16] Y. T. Sung, Y. Li, and J. E. Scharer, Phys. Plasmas **23**, 092113 (2016).

[17] Y. T. Sung, Y. Li, and J. E. Scharer, Phys. Plasmas **22**, 034503 (2015).

[18] K. Takahashi, H. Akahoshi, C. Charles, R. W. Boswell, and A. Ando, Phys. Plasmas **24**, 084503 (2017).

[19] N. Gulbrandsen and Å. Fredriksen, Front. Phys. **5**, 1–8 (2017).

[20] N. Singh, Phys. Plasmas **18**, 122105 (2011).

[21] K. Takahashi, C. Charles, R. Boswell, and R. Hatakeyama, Phys. Plasmas **15**, 074505 (2008).

[22] K. Takahashi, Rev. Mod. Plasma Phys. **3**, 3 (2019).

[23] K. Takahashi, C. Charles, R. Boswell, T. Kaneko, and R. Hatakeyama, Phys. Plasmas **14**, 114503 (2007).

[24] Y. Zhang, C. Charles, and R. Boswell, Phys. Plasmas **23**, 083515 (2016).

[25] E. E. Scime, P. A. Keiter, M. M. Balkey, J. L. Kline, X. Sun, A. M. Keesee, R. A. Hardin, I. A. Biloiu, S. Houshmandyar, S. Chakraborty-Thakur, J. Carr, Jr., and S. Sears, J. Plasma Phys. **81**, 345810103 (2014).

[26] D. S. Thompson, "Three-dimensional multispecies distribution functions in a plasma boundary with an oblique magnetic field," Ph.D. thesis (West Virginia University, 2018).

[27] R. M. Magee, M. E. Galante, N. Gulbrandsen, D. W. McCarren, and E. E. Scime, Phys. Plasmas **19**, 123506 (2012).

[28] T. K. Popov, M. Dimitrova, P. Ivanova, J. Kovacic, T. Gyergyek, R. Dejarnac, J. Stockel, M. Pedrosa, D. Lopez-Bruna, and C. Hidalgo, Plasma Sources Sci. Technol. **25**, 033001 (2016).

[29] V. I. Demidov, S. V. Ratynskaia, R. J. Armstrong, and K. Rypdal, Phys. Plasmas **6**, 350–358 (1999).

[30] V. I. Demidov, S. V. Ratynskaia, and K. Rypdal, Contrib. Plasma Phys. **41**, 443–448 (2001).

[31] F. Magnus and J. T. Gudmundsson, Rev. Sci. Instrum. **79**, 073503 (2008).

[32] P. Chabert and N. Braithwaite, *Physics of Radio Frequency Plasmas* (Cambridge University Press, 2011).

[33] V. Godyak, Phys. Plasmas **12**, 055501 (2005).

[34] F. F. Chen and D. Arnush, Phys. Plasmas **4**, 3411 (1997).

[35] K. Niemi and M. Krämer, Phys. Plasmas **15**, 073503 (2008).

[36] B. Clarenbach, M. Krämer, and B. Lorenz, J. Phys. D **40**, 5117–5129 (2007).

[37] P. A. Piotrowicz, J. F. Caneses, M. A. Showers, D. L. Green, R. H. Goulding, J. B. O. Caughman, T. M. Biewer, J. Rapp, and D. N. Ruzic, Phys. Plasmas **25**, 052101 (2018).

[38] F. F. Chen and D. Curreli, Phys. Plasmas **20**, 057102 (2013).

[39] D. Curreli and F. F. Chen, Phys. Plasmas **18**, 113501 (2011).

[40] C. Charles, Appl. Phys. Lett. **96**, 051502 (2010).

[41] X. Sun, "A study of ion acceleration, asymmetric optical pumping and low frequency waves in two expanding helicon plasmas," Ph.D. thesis (West Virginia University, 2005).

[42] A. Meige, R. W. Boswell, C. Charles, and M. M. Turner, Phys. Plasmas **12**, 052317 (2005).

[43] A. W. Molvik, A. R. Ellingboe, and T. D. Rognlien, Phys. Rev. Lett. **79**, 233 (1997).

[44] R. Chen and N. Hershkowitz, Phys. Rev. Lett. **80**, 4677 (1998).

[45] R. Hardin, "Measurement of short-wavelength electrostatic fluctuations in a helicon plasma source," Ph.D. thesis (West Virginia University, 2008).